PREDICTION OF AERODYNAMIC DERIVATIVES USING COMPUTATIONAL FLUID DYNAMICS (CFD) AT TRANSONIC SPEED

Article history
Received
12 February 2017
Received in revised form
31 July 2017
Accepted
15 August 2017

Norazila Othman[a*]
[a]Department of Aeronautics, Automotive and Ocean Engineering, Faculty of Mechanical Engineering, Universiti Teknologi Malaysia, 81310 UTM Johor Bahru, Johor, Malaysia

*Corresponding author
norazila@mail.fkm.utm.my

GRAPHICAL ABSTRACT

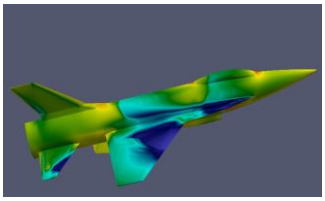

ABSTRACT

This paper aims to evaluate the aerodynamic derivatives from computational fluid dynamics to obtain derivatives at transonic speed. The derivatives are computed using the equation of Reynolds-Averaged-Navier-Stokes and a time-domain flow solver. In order to predict this study, standard dynamic model geometry is adopted. Three separated methods are used to calculate the aerodynamic derivatives. Then, the comparison betweenlow-fidelity solver, high-fidelity computational and experimental data available showedthat a satisfactory agreement was observed simultaneously. The study conducted showed the evaluation of unstable aerodynamic derivatives prediction, useful for longitudinal motion. The derivatives such as normal force derivatives and pitching moment derivatives function as important derivatives in the aerodynamic coefficient for the dynamic motion analysis.
This paper aims to evaluate the

KEYWORDS

Computational; Derivatives; Prediction; Transonic; Unsteady.

INTRODUCTION

Prediction of unsteady aerodynamic derivatives is the most important aspect for dynamic motion. Research in experiment and computation about predicting the aerodynamic derivatives had been done since the last ten years [1, 2]. However, there is a continued active research for computational method to establish the performance of the flow solver based estimation of aerodynamic derivatives, yet is not matured enough [3-4].

The visualization of flow is very important in order to know the effect from the aerodynamic derivatives via computational method. The close prediction of dynamic characteristics with experiment uses powerful tools of computational fluid dynamics (CFD) code [5]. Currently, CFD has made rapid progress and acquired many test cases environment to obtain the best agreement of aerodynamic databases compared to the experimental results [6]. Much effort had been put in computational technique to determine the aerodynamic derivatives and the coefficient in CFD around the world [7-9].

For example, in United States, the program called Computational Methods for Stability and Control (COMSAC) by NASA Langley Research Centre (LaRC) had investigated the capability of the high-fidelity CFD code for steady-state

derivatives computation [10]. Moreover, another application using CFD is Kestrel which was developed as a multi-physics analysis tool for fixed-wing aircraft in the framework of CREATE-AV model as explained in [3] which can simulate six degree-of-freedom aircraft motion with controlled surface motion and identify the nonlinear dynamic derivatives characteristics. On the other hand, in Europe, the simulation, stability and control research team (SimSAC)[11] had projects running simultaneously to enhance computerized environment such as CFD for aircraft synthesis and then integrated optimization methods (CEASIOM) [12]using the aerodynamic derivatives.

This paper presents the use of CFD to predict the aerodynamic derivatives for the specific transonic regime flow at Mach number 0.88 using the new-innovation CFD flow solver code called fast flow solver "FaSTAR". It was developed by Japan Aerospace and Exploration Agency (JAXA) [2-3, 6-7]. In order to use this flow solver, a full automatic grid generator "HexaGrid" was implemented. The moving grid method to the FaSTAR code was used to obtain the dynamic derivatives. The obtained results were compared for the steady and quasi-steady flow computations with experiment results. The analysis tools of CFD were validated among the existing CFD flow solver from previous publication and experimental results based on Deutsche ZentrumfürLuft-und Raumfahrt (DFVLR), National Aerospace laboratory (NAL), Japan and Fédération Française Aéronautique (FFA) with the basic model of standard dynamic model (SDM) [2-3, 6-7].

This paper is organized as follows: the target aircraft considered here is described in the following section. Then, the methodology, which contains an overview of the computational methods of aerodynamic derivatives, the estimation of static derivatives and dynamic derivatives are described, followed by theexplanation of the computational fluid dynamic toolsconsisting of the grid solver, flow solver and computational condition. Finally, the results and discussion are presented inclusive of the estimation of statics and dynamics derivatives at Mach number 0.88. The results also showed the comparison between CFD and experiments using DFVLR, NAL and FFA. Then, the conclusion is stated as the last remarks of this study.

TARGET AIRCRAFT

In this study, standard dynamic model (SDM) is used as the test aircraft model for CFD. As shown in Fig. 1, SDM has the moment of inertia I_{xx}, I_{yy} and I_{zz} of 0.125 kg.m^2, 0.539 kg.m^2, and 0.616 kg.m^2, respectively [2-3].

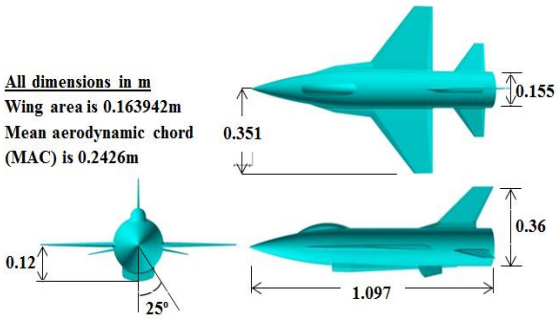

Figure 1. Three-view of SDM.

METHODOLOGY

Overview of Computational Methods of Aerodynamic Derivatives

The representation of the aerodynamic coefficient is normally modelled as the sum of several aerodynamic stability derivatives which is an inherent stability of an aircraft. The function needs to be multiplied with several effects which may vary depending on longitudinal flight conditions as shown in Eq. (1) [2]

$$C_i = f_1(\alpha,\beta,M,\delta) + f_2\left(\frac{\Omega c}{2U_\infty}\right) + f_3\left(\frac{\omega c}{2U_\infty}\right) \quad (1)$$

for $i = Z, X, M$

The first term on the right hand side can be obtained in static (steady) calculations, the second term can be measured from rotational balance (quasi-steady calculation) and third term from the forced oscillation (unsteady calculations), respectively. In this study, the aerodynamic coefficient databases using CFD are utilised. The prediction of aerodynamics derivatives were obtained using CFD through three separated

methods. First, is the estimation of static derivatives, second, is the estimation of steady rotated derivatives and third, the estimation of the unsteady derivatives.

Estimation of Static Derivatives

The first method is using static computation which produces the derivatives such as $C_{Z\alpha} \equiv \frac{\partial C_Z}{\partial \alpha}$ and $C_{M\alpha} \equiv \frac{\partial C_M}{\partial \alpha}$. The derivatives are obtained by calculating the central difference between the values of the corresponding angle of attack α_0.

$$\frac{\partial f(\alpha, C_Z)}{\partial \alpha} \approx \frac{f(\alpha + \Delta\alpha, C_Z) - f(\alpha - \Delta\alpha, C_Z)}{2\Delta\alpha} \tag{2}$$

Estimation of Steady-Rotated Derivatives

The second method is using the quasi-steady (steady rotated) method which produces the derivatives such as $C_{Zq} \equiv \frac{\partial C_Z}{\partial q}$ and $C_{Mq} \equiv \frac{\partial C_M}{\partial q}$ individually, where the term $C_{Z\dot{\alpha}} \equiv \frac{\partial C_Z}{\partial \dot{\alpha}}$ and $C_{M\dot{\alpha}} \equiv \frac{\partial C_M}{\partial \dot{\alpha}}$ are assumed as zero. In this estimation, the grid moving method is used.

Estimation of Dynamic Derivatives

The third method is using unsteady computational method which will obtain the derivatives of $C_{Zq}+C_{Z\dot{\alpha}}$ and $C_{Mq}+C_{M\dot{\alpha}}$ simultaneously. These summations of derivatives cannot be predicted individually [14-15]. For the evaluation of unsteady dynamic model, the moving grids method is used.

In dynamic motion, the dampness and stiffness derivatives are very important. The results obtained from the static methods analysis are used as a starting value. As an example, C_M is estimated from the non-linear approximate equation as in Eq. (1). Then, the derivation of Eq. (1) yields the linear approximate equation as in Eq. (3). Using the same method, C_Z and C_X are calculated in the same way as C_M.

$$C_m = C_{mo} + C_{m\alpha}\alpha + \left(C_{mq} + C_{m\dot{\alpha}}\right)\frac{c_{ref}}{U}\dot{\alpha} \tag{3}$$

Then, $\alpha = \theta \sin(\omega t)$ is substituted in Eq. (3) to obtain Eq. (4) as follows.

$$C_m = C_{mo} + A\sin(\omega t + \varepsilon) \tag{4}$$

where,

$$A = \sqrt{{C_{m\alpha}}^2 + (C_{mq} + C_{m\dot{\alpha}})^2\left(\frac{c}{U}\right)^2 \omega^2\theta}$$

$$\tan\varepsilon = \left(C_{mq} + C_{m\dot{\alpha}}\right)\left(\frac{c}{U}\right)\omega \cdot \frac{1}{C_{m\alpha}}$$

where, A and ε are identified from the result obtained from the means of the least square method. Therefore, $C_{M\alpha}$ and $(C_{Mq}+C_{M\dot{\alpha}})$ are calculated using Eq. (5) and Eq. (6).

$$C_{m\alpha} = \frac{A}{\theta}\cos\varepsilon \tag{5}$$

$$\left(C_{mq} + C_{m\dot{\alpha}}\right) = \frac{U}{c_{ref}}\frac{A}{\theta\omega}\sin\varepsilon \tag{6}$$

Computational Fluid Dynamics Tools

Computational Solver

Grid Solver

In this study, the unstructured hexahedral mesh is generated around SDM using HexaGrid software [2-3].

Firstly, the Cartesian typegrid is generated for local refinement. The step starts from one cell to cover the whole computational domain, which is set by the users. In the three-dimensional space, each refinement will be divided iso tropically into eight child cells of equal size and shape. After that, the local grid will be refined until the size of connecting cells to be the solid surface that is smaller than a maximum grid size set by users. This process is automatically refined according to the surface grid size as shown in Fig. 2(1). Next, the grid will be refined continuously until the size of cells connecting the solid surface with the large curvature reaching either a satisfactory level or a minimum grid size set by users as shown in Fig.

2(2). After, the Cartesian grid cells intersect the solid object, this grid is snapped onto the solid surface by moving each node of a quad surface to the closest location on the solid surface. A number of prismatic grid layers is constructed on the snapped surface. Users can define the thickness of the first grid layer, and the expansion factor of thickness. The benefit of using this method is users can control the grid size using the "Refinement box" with HexaGridGUI as shown in Fig. 2(3). Generally, in this study, the cell size is set uniformly to a value of 1.6 mm, and this size generates approximately about 165 cells for the mean aerodynamic chord (MAC). The thickness of the first grid layer is 0.02 mm and corresponds to the y+=7[16-17]. Therefore, for the longitudinal motion, such as pitching moment motion uses the half span model with about 7 million cells in a base grid model and 23 million cells for fine grid as shown in Fig. 3(a)-(b).

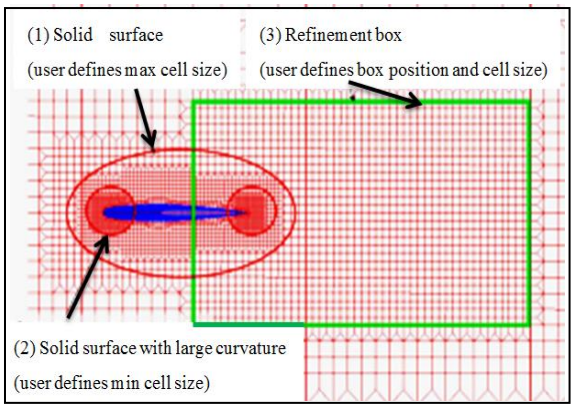

Figure 2: Refinement process of Cartesian grid.

(a)

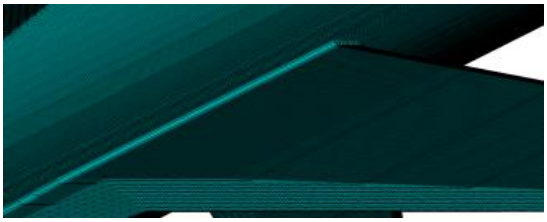

(b)

Figure 3: Computational grid. (a) Base grid, (b) Fine grid.

Flow Solver

The CFD flow solver used is called FaSTAR. FaSTAR was developed by the Japan Aerospace Exploratory Agency (JAXA). FaSTAR is performed using unstructured high speed networks. The compressible Navier-Stokes equation is employed as the governing equation. Spalart-Almaras with rotation correction turbulence model (SA-R) [18] is used as a turbulent model. Then, the finite volume method (VLM) is employed for space visualization. In order to evaluate numerical functions, the Harten-Lax-Van-Leer-Einfeldt-Wada (HLLEW) [19] is employed. Second-order spatial accuracy is realized by using MUSCL interpolation [20]. The gradients at cell interfaces are reconstructed using a Green-Gauss (GG) method and a Venkatakrishnan limiter [21] extended for unstructured grids is used. A dual-time stepping method is used to perform accurate time calculations [22]. Lower/upper symmetric Gauss-Seidal (LU-SGS) [23] implicit method is used for the pseudo time sub-iteration, and the physical time is discretized by three-point backward difference scheme.

In moving grids method, the movement speed of grids is added to the flux which passes through the cell boundary. Static rotation analysis yields constant rotation speed. Dynamic motion analysis yields movement grids to simulate rotation speeds and time variation of angle of attack α_0. In dynamic motion analysis, the dual time stepping method using quasi-time is introduced. Inertia was evaluated through second-order backward scheme. The time step of quasi-time used the local time stepping method and diagonal component of LU-SGS implicit method as shown in Eq. (7).

$$D_i = \sum_{j\in i}\left\{V_i\left(\frac{3}{2\Delta t}+\frac{1}{\Delta\tau}\right)+\frac{1}{2}\sum_{j\in i}\rho_{Aj}S_j\right\}I = \sum_{j\in i}\left(V_i\frac{3}{2\Delta t}+\frac{\rho_A}{CFL}+\frac{1}{2}\sum_{j\in i}\rho_{Aj}S_j\right)I \quad (7)$$

where i is cell number , j is surface number, V is volume, Δt is time, $\Delta\tau$ is quasi-time, ρ_A is maximum characteristics of value of Jacobian and S is area

of cell surface. Therefore, the usage of $\Delta t$is 0.1 and the time step is iterated about 10000 steps using a period of vibration [16-18].

Computational Condition

In this study the computational conditions are carried out using several wind tunnels data such as DFVLR, FFA and NAL. Thus, the comparison results, specifically in Reynolds numberare *Re* = 2.82×10^6 and Mach number *Ma* = 0.88. The test case is without shock wave and the reduced frequency, *k* = $\omega c/U$ = 0.0457, where ω = is the angular frequency and U is uniform flow velocity. However, this reduced frequency takes a long time for integration. The ratio of time scale is $\frac{T_1}{T_2}=\frac{1/f}{2\pi/\omega}{c_{ref}}/U$ which is approximately about 120. This indicates that the flow passes 120 times over the wing during a period. The simulation of the dynamic motion is half amplitude θ =1.0°. The CFL number is about 50 and inner iteration is 50. For unsteady computation, the Unsteady Reynolds-Averaged Navier-Stokes Simulation (URANS) is employed. URANS is employed to obtain the historical data for a long time.

Results and Discussion

In this study, the evaluation is only done for longitudinal motion. The result showed that normal coefficient C_{Z}, axial coefficient C_{X} and pitching moment coefficient C_{M} is consistent with the experimental data DFVLR when the angle of attack was increased.

Estimation of Static Derivatives

The simulation for steady motion is analysed based on steady flight motion at speed U and angle of attack α_0. In Fig. 4 the pressure coefficient *Cp* contours for steady flow characteristics were shown from the angle of attack 0.0°to 20.0°. Based on Fig. 4(a), the vortex flow does not occur at the leading edge of wing at angle of attack 0.0°. By increasing the angle of attack to 20.0°, the leading edge surface angle will also increase, consequently increasing the front flow occurring at the vortex. In this condition, aircraft has less pressure and influences stall flight due to the loss lift up. Hence, aircraft must be extra careful to fly due to the change in the vortex flow such example in Fig. 4(e).

Fig. 5(a) shows the C_{Z} plot against the angle of attack, Fig. 5(b) shows C_{X} plot against the angle of attack and Fig. 5(c) shows C_{M} plot against the angle of attack. Based on Fig. 5(a) and (b),$C_{\mathrm{Z}}$and C_{X} from DFVLR's and FFA's experiment and the results from CFD are consistent for both steady and unsteady computation. DATCOM result showed a higher value than the other results. C_{M} from CFD almost agrees with that obtained from the NAL's and DFVLR's experiment for the value of angle attack α between 0.0° to 10.0°. However, when comparing the CFD results with increased angle of attack, the same plot trend only appears for angle of attack value of up to 15.0°, otherwise, C_{M} value for CFD will drop drastically compared to the data of DFVLR and FFA. DATCOM results are considered acceptable because they are still in the range of prediction [2].

From the obtained aerodynamic coefficient (Fig 5(a)-(c)), the stiffness derivatives namely $C_{\mathrm{Z}\alpha}$, $C_{\mathrm{X}\alpha}$and $C_{\mathrm{M}\alpha}$are calculated using central difference method. In Fig. 6(a)-(c) the stiffness derivatives of$C_{\mathrm{Z}\alpha}$,$C_{\mathrm{X}\alpha}$and $C_{\mathrm{M}\alpha}$for steady and unsteady computation are shown respectively. Based on Fig. 6(a), the CFD steady computation has large values of$C_{\mathrm{Z}\alpha}$compared to experiment NAL, but closer to DFVLR. Moreover, in Fig. 6(b) and (c), $C_{\mathrm{X}\alpha}$ and $C_{\mathrm{M}\alpha}$ also showed that the result of steady CFD computation was far different from the result of experiment NAL data.

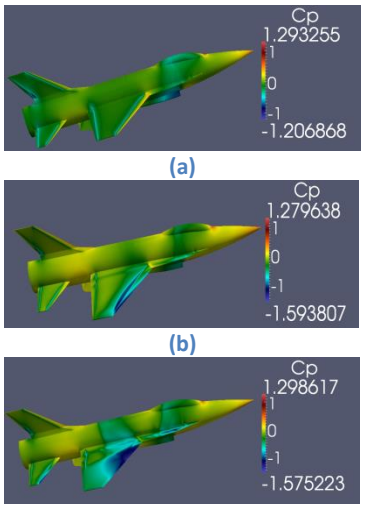

(c)

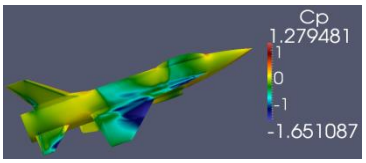

(d)

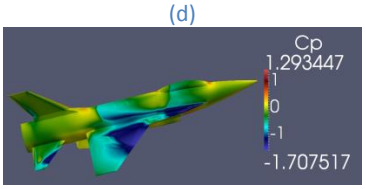

(e)

Figure 4. *Cp* contours with Mach number = 0.88 for steady flow characteristics. (a) Angle of attack = 0.0 degree, (b) Angle of attack = 5.0 degrees, (c) 10.0 degrees, (d) 15.0 degrees, (e) 20.0 degrees.

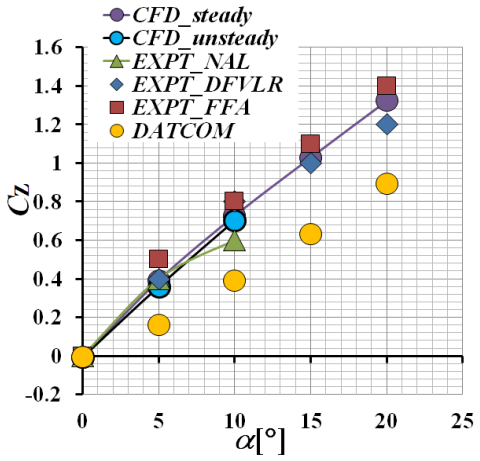

(a)

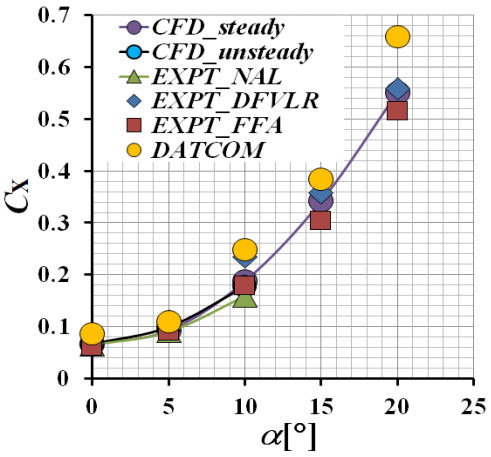

(b)

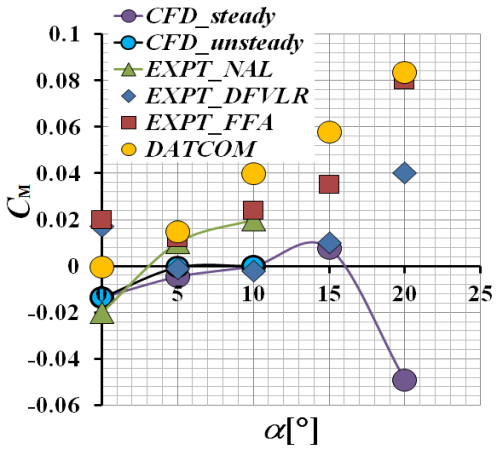

(c)

Figure 5. Comparison of steady characteristics model, CFD, DATCOM and experiment results at variousangles of attack. (a) Normal force coefficient C_Z, (b) axial force coefficient, $C_X$and (c) pitching moment coefficient C_M.

Based on Fig. 6(a)-(c), the unsteady derivatives method for $C_{Z\alpha}$, $C_{X\alpha}$and $C_{M\alpha}$showed better agreement with the experimental results [2]. Based on Fig. 6(a), the$C_{Z\alpha}$of unsteady computation has a closer values compared to steady computation when compared with the experiment NAL. In addition, the comparison of $C_{M\alpha}$ for steady and unsteady computation proved that the unsteady computation agree well with the experiment NAL as shown in Fig. 6(c). The same trend for unsteady methods showed close prediction between CFD and experiment NAL for $C_{X\alpha}$. However, the comparison between experimental data, such as DFVLR and FFA does not agree well. This may be caused by the difference in Reynolds number value and CFL number.

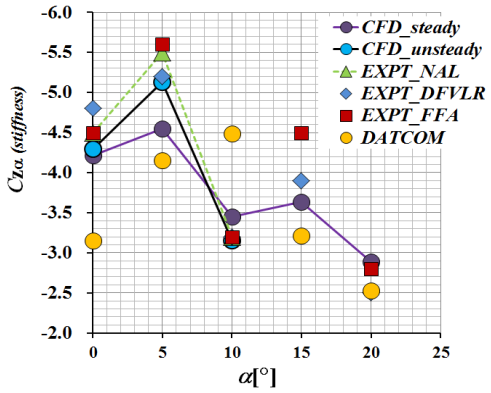

(a)

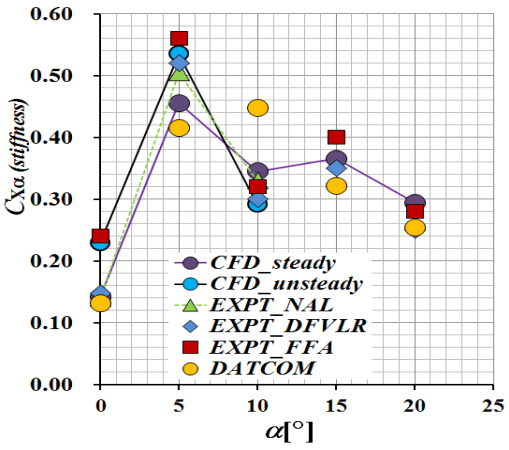

(b)

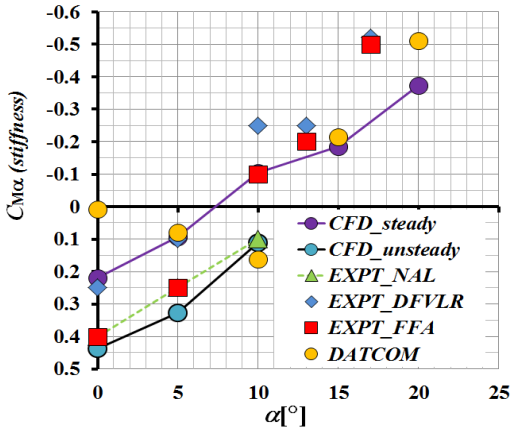

(c)

Figure 6. Comparison of stiffness derivatives among CFD, DATCOM and experiment results. (a) $C_{Z\alpha}$versus angle of attack, (b) $C_{X\alpha}$versus angle of attack, and (c) $C_{M\alpha}$versus angle of attack.

Estimation of Dynamic Derivatives

Next, based on Fig. 7, the results showed the dynamic derivatives data. The dynamic derivatives were computed in two ways which are using quasi-steady rotational method and unsteady method. For quasi-steady rotational method the rotational derivatives such as C_{Zq} and C_{Mq} can be computed individually and$C_{Z\dot{\alpha}}$ and$C_{M\dot{\alpha}}$are assumed as zero. Therefore, the damping derivatives ($C_{Zq}$and C_{Mq}) are decreased at a higher angle of attack. On the other hand, in the dynamic motion analysis, the damping derivatives are increased at a higher angle of attack. From these results, the dynamic motion using unsteady method analysis is better than steady analysis. According to Fig. 7(a), the dynamic derivatives for normal coefficient such asC_{Zq} are positive values. However, when computed using the unsteady methods, the values of $C_{Zq}+C_{Z\dot{\alpha}}$ are computed together, then the results were much closer to the experiment NAL. This value also shows the same trend results when compared to the DFVLR and FFA. Furthermore, in Fig. 7(b), the same situation occurs for C_{Mq}. The singular evaluation of C_{Mq}gives far prediction from the experiment NAL and the trend data samples of course do not agree well. However, using unsteady computation, the results of CFD were the total values of $C_{Mq}+C_{M\dot{\alpha}}$,which was good enough compared to the NAL data and the close trend with the DFVLR and FFA. In this analysis $C_{Xq}$is neglected as it is very small and the unsteady flow method is not applied.

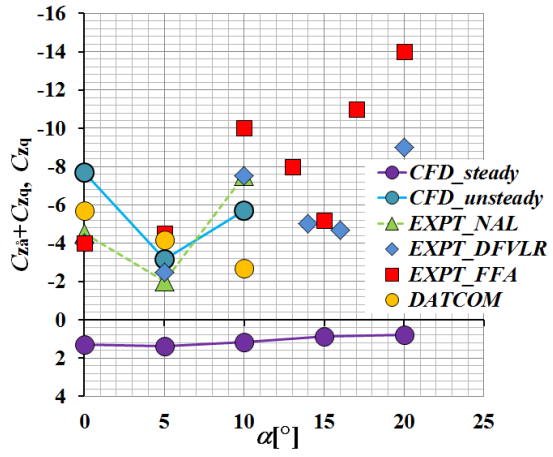

(a)

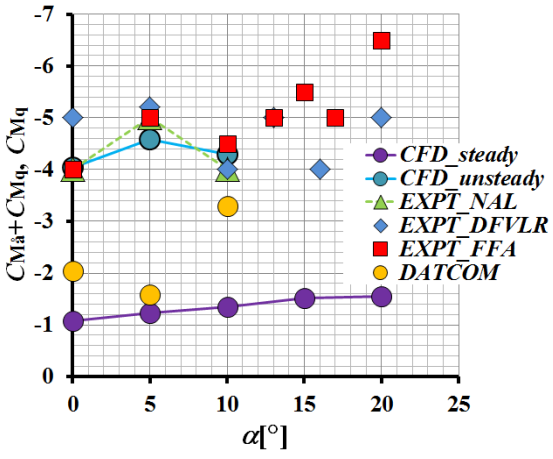

(b)

Figure 7. Dynamic derivatives among CFD version and experiment result. (a) $C_{Zq}+C_{Z\dot{\alpha}}$versus angle of attack and (b)$C_{Mq}+C_{M\dot{\alpha}}$ versus angle of attack.

Simulation of Longitudinal Motion

The simulation of longitudinal motion can be observed by obtaining the longitudinal mode.

There are two longitudinal modes which are long-period mode and short-period mode. First, results from aerodynamic derivatives used unsteady derivatives. The observation of mode motion is shown in Fig. 8. The comparison between the results from the DATCOM, CFD data and the experimental result by FFA were made for angle of attack 0.0° and Mach number 0.88. Fig. 8(a) shows the comparison of long-period mode motion and Fig. 8(b) shows the short-period mode motion. In this comparison, the CFD results were almost similar to the experiment motion, while the DATCOM is slightly different as shown in both figures 8(a) and (b). This reason proves that the prediction from CFD showed the accurate value for the prediction that can be a useful comparison to the experiment task.

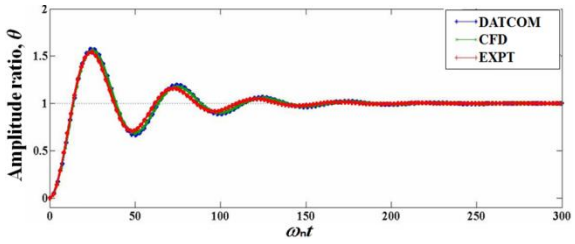

(a)

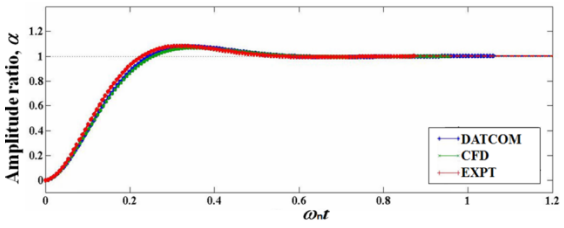

(b)

Figure 8. Comparisonsof longitudinal motionbetween the results from the low-fidelity aerodynamics (DATCOM), the high-fidelity CFD and the experimental data.**(a)** long–period mode motion affected by pitch angle, ϑ and(b) short–period mode motion from angle, α.

Conclusions

This study concludes that the solution to calculate aerodynamic coefficient and derivatives for SDM at transonic condition Mach number 0.88 was successful using HexaGrid and FaSTAR CFD flow solver. Normal coefficient, axial coefficient and pitching moment coefficient showed good agreement with the experimental data DFVLR with strong shock wave and vortexes when the angle of attack was increased. Compared to the existing study result and wind tunnel data, it was found that the dynamic motion (unsteady) analysis showed greater agreement than steady (static) motion for the aerodynamic derivatives analysis, since $C_{z\dot{\alpha}}$ and $C_{m\dot{\alpha}}$ play an important role for the dynamic motion analysis. According to the flow field visualization, wing-tip vortex and wake of the main wing were influenced by pitching motion. Therefore, pitching motion analysis assured the time convergence required by pertinent inner iteration.

Acknowledgements

This work is supported by Asian Human Resources Fund (AHRF) from Tokyo Metropolitan Government to the Tokyo Metropolitan University (TMU), Japan.

Nomenclature

C_{M} : Pitching moment coefficient.
C_{X} : Axial coefficient.
C_{Z} : Normal coefficient.
$C_{\mathrm{M}\alpha}$: Pitching moment coefficient due to angle of attack.
$C_{\mathrm{X}\alpha}$: Axial coefficient due to angle of attack.
$C_{\mathrm{Z}\alpha}$: Normal coefficient due to angle of attack.
$C_{\mathrm{M}\dot{\alpha}}$: Pitching moment due to time rates of angle of attack.
$C_{\mathrm{M}q}$: Pitching moment coefficient due to pitch rate.
$C_{\mathrm{Z}q}$: Normal coefficient due to time rates of angle of attack.
$C_{\mathrm{Z}\dot{\alpha}}$: Normal coefficient due to pitch rate.

References

[1] *Ueno, M., and Miwa, H., 2001. New Dynamic Stability Equipment for Transonic Wind Tunnel Testing at NAL, 39th AIAA Aerospace Sciences Meeting and Exhibit, Reno, NV.*

[2] *Hashimoto, A., Hashizume, M., Sunada, S., Ueno, M., Murakami, K., 2013.Unsteady Analysis of Aerodynamic Derivatives on Standard Dynamic Model. 51st AIAA Aerospace Sciences Meeting including The New Horizons Forum and Aerospace Exposition, Grapevine (Dallas/Ft. Woth Region), Texas.*

[3] Narita, Y.,Hashimoto, A.,Kanazaki, M., 2012.Numerical Simulation: Flight Dynamics Stability Analysis using Unstructured Based Navier-Stokes Solver. Asia-Pacific International Symposium on Aerospace Technology (APISAT 2012), Korea.

[4] Cristofaro, M.,WangY., and Ronch, A. Da., 2014.TowardsComputational Flight Dynamics of APassengers Jet Aircraft. 29th Congress of the International Council of the Aeronautical Sciences, ICAS 2014, St.Petersburg, Russia.

[5] Salas,M. D., 2006. Digital Flight: The Last CFD Aeronautical Grand Challenge.Journal of Scientific Computing. 28: No.2/3.

[6] Murayama, M., Yamamoto, K., Hashimoto, A., Ishida, T., Ueno. M., Tanaka, K., Ito, Y., 2013. Summary of JAXA Studies for the AIAA CFD Drag Prediction Workshop Using UPACS and FaSTAR.

[7] Hashimoto, A., Murakami, K., Aoyama, T., et al, 2012. Development of FAST Unstructured CFD Code "FaSTAR". ICAS 2012.

[8] Ronch, A. Da.,Ghoreyshi, M., and Badcock, K. J., 2011. On the Generation of Flight Dynamics Aerodynamics Tables by Computational Fluid Dynamics. Progress in Aerospace Sciences. 47:8:597-620.

[9] Ronch, A. Da.,Vallespin, D., 2012. Evaluation of Dynamic Derivatives Using Computational Fluid Dynamics. AIAA Journal. 50:2:470-484.

[10] Park, M. A., Green, L. L., 2000. Steady-State Computation of Constant Rotational Rate Dynamic Stability Derivatives. 18th Applied Aerodynamics Conference. AIAA 2000-4321.

[11] Grabowski, T. G., MieszalskiD.,andMarcinkiewicz, E., 2011.Stability Analysis Using SDSA Tool. Progress in Aerospace Sciences. 47: 636-646.

[12] Rizzi, A., 2011.Modeling and Simulating Aircraft Stability and Control-The SIMSAC Project. Progress in Aerospace Sciences 47: 573-588.

[13] Zhengjie, W.,Zhijun, L.,NingjunF., and Meifang, G., 2013. Flight Dynamics Modelling of A Small Ducted Fan Aerial Vehicle Based on Parameter Identification. Chinese Journal of Aeronautics. 26:6:1439-1448.

[14] Hashimoto, A., Hayashi, K., Ishiko, K.,Murakami, K.,Aoyama, T.,Tagai, R.,KogaS.,and Nagai, S., 2014.Dynamic Stability Analysis of Reentry Capsule with Detached-Eddy Simulation. 11th World Congress on Computational Mechanics, 5th European Conference on Computational Mechanics and 6th European Conference on Computational Fluid Dynamics, Barcelona, Spain.

[15] Schmit, E., 1985.Standard Dynamics Model Experiments with The DFVLR/AVA Transonic Derivative Balance. AGARD-CP-386 Ref. No. 2.

[16] Hashimoto, A., Murakami, K.,Aoyama, T.,Lahur, P. R., 2009. Lift and Drag Prediction Using Automatic Hexahedra Grid Generation Method. AIAA 2009-1365.

[17] Lahur, P. R., 2005.Automatic Hexahedra Grid Generation Method for Component-Based Surface Geometry, AIAA005-5242.

[18] Spalart, R. R., and Allmaras, S. R., 1992. A One-Equation Turbulence Model for Aerodynamic Flows. 30th Aerospace Sciences Meeting and Exhibit, Reno, Nevada. AIAA 1992-0439.

[19] Fureby, C., 2008. Towards the Use of Large Eddy Simulation in Engineering. Progress in Aerospace Sciences. 44:381-396.

[20] Shima, E., Kitamura, K., Fujimoto, K., 2010. New Gradient Calculation Method for MUSCL Type CFD Schemes in Arbitrary Polyhedra. 48th AIAA Aerospace Sciences Meeting Including the New Horizons Forum and Aerospace Exposition, AIAA 2010-1081.

[21] Hishida, M., Hashimoto, A., Murakami, K., Aoyama, T., 2010. A New Slope Limiter for Fast Unstructured CFD Solver FaSTAR. 42thFluid Dynamics lecture/Aerospace Numerical Simulation Symposium.

[22] Visbal, M. R., and Gordnier, R. E., 2000. A High-Order Flow Solver for Deforming and Moving Meshes. Fluids Conference and Exhibit, Denver, CO. AIAA 2000-2619.

[23] Sharov, D., and Nakahashi, K., 1998. Reordering of Hybrid Unstructured Grids for Lower/Upper Symmetric Gauss-Seidel Computations. AIAA Journal: Technical Notes. 36:3:484-486.